Biochimica et Biophysica Acta 1852 (2015) 2402–2413

Contents lists available at ScienceDirect

Biochimica et Biophysica Acta

journal homepage: www.elsevier.com/locate/bbadis

Downregulation of STIM2 improves neuronal survival after traumatic brain injury by alleviating calcium overload and mitochondrial dysfunction

Wei Rao [1], Lei Zhang [1], Cheng Peng [1], Hao Hui [1], Kai Wang, Ning Su, Li Wang, Shu-hui Dai, Yue-fan Yang, Tao Chen, Peng Luo, Zhou Fei *

Department of Neurosurgery, Xijing Hospital, Fourth Military Medical University, Xi'an 710032, PR China

ARTICLE INFO

Article history:
Received 28 April 2015
Received in revised form 28 July 2015
Accepted 19 August 2015
Available online 20 August 2015

Keywords:
Traumatic brain injury
Neurons
SOCE
Mitochondria dysfunction
Calcium homeostasis

ABSTRACT

Although store-operated calcium entry (SOCE) has been implicated in several neurological disorders, the exact mechanism for its role in traumatic brain injury (TBI) has not been elucidated. In this study, we found that TBI upregulated the expression of a calcium sensor protein called stromal interactive molecule 2 (STIM2); however, the levels of its homologue, STIM1, were unaffected. Both STIM1 and STIM2 are crucial components of SOCE, both in vivo and in vitro. Using shRNA, we discovered that downregulation of STIM2, but not STIM1, significantly improved neuronal survival in both an in vitro and in vivo model of TBI, decreasing neuronal apoptosis, and preserving neurological function. This neuroprotection was associated with alleviating TBI-induced calcium overload and preserving mitochondrial function. Additionally, downregulation of STIM2 not only inhibited Ca^{2+} release from the endoplasmic reticulum (ER), but also reduced SOCE-mediated Ca^{2+} influx, decreased mitochondrial Ca^{2+}, restored mitochondrial morphology and improved mitochondrial function, including MMP maintenance, ROS production and ATP synthesis. These results indicate that inhibition of STIM2 can protect neurons from TBI by inhibiting calcium overload and preserving mitochondrial function. This suggests that STIM2 might be an effective interventional target for TBI.

1. Introduction

Traumatic brain injury (TBI) is the most common neurological disease, and as such, has become a significant public health problem [1–3]. Primary injuries trigger complex cascades of secondary injury processes, which can persist for hours, days, and even months following an injury. Most treatments for TBI are aimed at ameliorating these secondary insults [4,5]. Disturbance of calcium homeostasis, dysregulation of calcium regulatory proteins and/or mitochondrial dysfunction have been extensively associated with the development of secondary injuries in neuronal cells after TBI. These secondary injuries can lead to serious neurological dysfunction and even death [6,7]. Therefore, it is of crucial importance that we investigate the mechanisms of calcium dysregulation in TBI, as well as other neurological conditions.

Store-operated calcium entry (SOCE), which has been extensively studied in non-excitable cells, is mediated by sensor proteins called stromal interactive molecules (STIM) and also by Ca^{2+} release-activated Ca^{2+} channels (CACs) [8]. The two known STIM proteins, STIM1 and STIM2, are distributed mainly on the endoplasmic reticulum (ER) and are the crucial regulators of SOCE. These proteins function by sensing the Ca^{2+} concentration in the ER lumen and mediating extracellular Ca^{2+} entry to raise cytosolic Ca^{2+} to refill Ca^{2+} stores. Numerous studies have demonstrated that SOCE is linked with Ca^{2+} homeostasis in non-excitable cells [8,9]. Recently, a role for SOCE has been found in excitable cells as well, particularly in neurons, where SOCE has been found to regulate synaptic plasticity, neurotransmitter release, and gene expression [10–13]. Moreover, SOCE has also been implicated in several neurological disorders, including Alzheimer's disease (AD), Huntington's disease (HD), chronic epilepsy, painful nerve injury and cerebral ischemia [10,14–16]. Interestingly, the different disorders seem to be mediated differentially by the STIM family members [17]. For example, Zeiger W. et al. found that STIM1-mediated SOCE reduced amyloid peptide secretion in AD [18], while Sun S.Y. et al. established that reduced synaptic STIM2-mediated SOCE causes destabilization of mature spines in AD [10]. Additionally, STIM2 regulated SOCE in

Abbreviations: Alzheimer's disease, AD; Amyotrophic lateral sclerosis, ALS; Anterior–posterior, AP; Apoptotic index, AI; Area under the curve, AUC; Ca^{2+} release-activated Ca^{2+} channels, CACS; Controlled cortex injury, CCI; Dorsal–ventral, DV; Endoplasmic reticulum, ER; Huntingdon's disease, HD; Lactate dehydrogenase, LDH; Medial–lateral, ML; Metabotropic glutamate receptor, mGluR1; Mitochondrial membrane potential, MMP; Parkinson's disease, PD; Reactive oxygen species, ROS; Store-operated calcium entry, SOCE; Stromal interactive molecule 2, STIM2; Tetramethylrhodamine, TMRM; Traumatic brain injury, TBI; Traumatic neuronal injury, TNI; Trifluorocabonylcyanide phenyhydrazone, FCCP; TdT-mediated dUTP Nick End-Labeling, TUNEL.

* Corresponding author.
E-mail address: feizhou@fmmu.edu.cn (Z. Fei).

[1] These authors contributed equally to this work.

http://dx.doi.org/10.1016/j.bbadis.2015.08.014
0925-4439/

neurons and knockout of STIM2 protected neurons from hypoxic neuronal cell death [14]. However, whether and how STIM1- or STIM2-mediated SOCE has effects in neuronal injury induced by TBI has not been elucidated.

In this study, we used a scratch model in vitro and a controlled cortex injury (CCI) model in vivo to mimic TBI and explore the mechanism of SOCE in TBI. These results uncovered an important role of STIM2-mediated SOCE in TBI induced calcium overload and mitochondrial dysfunction. Inhibition of STIM2, but not STIM1, protected neurons from TBI-induced injury. This neuroprotection might partially be due to a decrease in TBI-induced calcium overload and reservation dynamics, as well as a preservation of mitochondria function. Therefore, STIM2 and STIM2-mediated SOCE might be an important intervention target in TBI.

2. Materials and methods

2.1. Animals

Mature male (10–12 weeks, 25–28 g) and embryonic (14–15 d) C57BL/6 mice were obtained from The Experimental Center of Fourth Military Medical University. The mice were kept at a constant temperature (approximately 27 °C) in an air-conditioned room and were exposed to a 12-h light/dark cycle. All animal studies were performed in adherence to the National Institutes of Health Guidelines on the Use of Laboratory Animals, and were approved by the Fourth Military Medical University Committee on Animal Care.

2.2. Cortical neuronal culture

Primary cortical neurons were prepared from embryonic 14–15 d C57BL/6 embryos as previously described [19]. Briefly, cortices of mouse embryos were dissected and minced, followed by a 30 minute incubation at 37 °C in Ca^{2+}/Mg^{2+}-free HBSS containing 15 U/ml papain solution (Worthington, Lakewood, NJ, USA) and 0.2 mg/ml DNase I (Beyotime, Haimen, China). The cells were re-suspended in a neurobasal medium supplemented with 2% B27 supplement and 0.5 mM L-GlutaMax™-I (Gibco, MD, USA) and plated onto poly-L-lysine (Sigma-Aldrich, MO, USA) coated dishes at a density of 2.5×10^5 cells/cm^2. After 7–10 days of culture, the cells were used for experiments.

2.3. Traumatic injury model on cultured neurons

Traumatic neuronal injury (TNI) was performed according to Mukhin's method [20], with some modifications. In brief, traumatic injury was performed on cultured neurons by using a rotating scribe injury device, which consisted of a rotating cylinder with ten holes, steel needles and a permanent magnet. The cylinder holes are distributed at the same interval from the center, and these holes allowed the ten steel needles to freely cross through. A magnet is placed under the culture dish, which ensured that the steel needles could cling to the cell layer as the cylinder rotated. After one turn of this device, ten concentric circular scratches were produced in the neuronal layer with equal distances (1.5 mm) between the scratches. This model, and its variants, are highly reproducible and are able to induce severe TNI [21–24].

2.4. Animal models

For in vivo studies, TBI was produced in mice by using a Pinpoint™ Precision Cortical Impactor (PCI3000; Hatteras Instruments, Cary, NC, USA) in accordance with previous methods [25]. For the surgeries, standard presurgical preparations were followed under sterile conditions. Briefly, mice were anesthetized with isoflurane in oxygen (4% for induction, 2.5% for maintenance) and the animals were placed in the stereotaxic frame. After incising the scalp, a craniotomy was performed using a dental drill with a trephine bit (ø = 3 mm) on the left motor cortex (anterior–posterior (AP) −2 mm, medial-lateral (ML) 2.0 mm from bregma). During the procedure, considerable care was taken to avoid additional injury to the dura. To induce injury, a metal tip (ø = 2.5 mm) was angled vertical to the cortex surface at the center of the craniotomy. The tip was then lowered to touch the cortex surface, initially using coarse adjustment and then, as it got closer to the cortex, fine adjustment, as determined by an electronic continuity sensor. Once the machine was adjusted properly, the TBI was induced using the PCI3000 by retracting the tip upward by 2 cm, and then a down stroke (velocity: 1.5 m/s, deformation depth: 1.5 mm, duration: 120 ms). Immediately after the injury, the wound was tightly sutured closed and the mice were returned to cages where water and food were freely available.

2.5. Plasmids and lentivirus generation

Optimal STIM1 shRNA (5′-GCA GTA CTA CAA CAT CAA GAA-3′), STIM2 shRNA (5′-GAC GAA GTA GAC CAC AAG ATT-3′) or scramble shRNA (5′-UUC UCC GAA CGU GUC ACG U-3′) was cloned into the lentivirus-based RNAi vector pGCL vector. Its sequence was confirmed using PCR and sequencing analysis. Lentivirus preparations were produced by the Shanghai GeneChem, Co. Ltd., China. Primary neurons were infected by adding lentivirus particles to the neuronal cultures at an MOI of approximately 30. Forty-eight hours after infection, primary neurons were used for experiments.

2.6. Real-time RT-PCR

After treating the neurons or the mice as indicated for each experiment, total RNA was extracted from neurons or cortexes using a MiniBEST Universal RNA extraction kit (Takara, Dalian, China) according to the manufacturer's protocols. 2 μg of template RNA was used to synthesize cDNA using a reverse transcription kit (Takara, Dalian, China). Quantitative RT-PCR was performed using CFX-96 (Bio-Rad, Los Angeles, CA, USA). Specificity of the amplified product was confirmed by examination of dissociation plots and gel electrophoresis. The following primers were used for real-time PCR: STIM1: forward, 5′-TGA GGC CGT CCG AAA CAT C-3′; reverse, 5′-TCA CTG TTG GGT CAT GGT AAT TGA G-3′; STIM2: forward, 5′-TCT GTC CCT GAC GCA CTA CAG AA-3′; reverse, 5′-ACG TGC AGG GTC CCA AAG A-3′;GAPDH: forward, 5′-GGG TCA GAA GGA TTC CTA TG-3′; and reverse, 5′-GGT CTC AAA CAT GAT CTG GG-3′. Samples were tested in triplicate, and data from four independent experiments were used for analysis. Relative gene expression was calculated using the $2^{-\Delta\Delta CT}$ method [26].

2.7. Western blot

Western blots were analyzed as previously described [27]. After treating the neurons or the mice as indicated for each of the experiments, proteins were extracted from neurons or cortexes using a RIPA lysis buffer supplemented with protease inhibitors (Roche Applied Bioscience, Indianapolis, IN, USA). Protein concentration was quantified using a BCA protein kit (Thermo Scientific, USA). Equal amounts of proteins were loaded on 8–12% SDS-PAGE gels. After electrophoresis, the proteins were transferred to nitrocellulose membranes. The membranes were then blocked with 5% skim milk and incubated at 4 °C overnight with the appropriate primary antibody: STIM1, 1:2000; STIM2, 1:1000; β-actin, 1:2000 (CST, Danvers, MA, USA). The blots were then incubated with horseradish peroxidase-conjugated secondary antibodies (1:20,000, CST, MA, USA), followed by incubation with a chemiluminescent substrate (Thermo Scientific, USA) and were detected on film. Western blots for each protein were repeated three times. The optical densities of the protein bands were calculated using a MiVnt image analysis system (Bio-Rad, CA, USA), and the results of the three bands were averaged.

2.8. Lactate dehydrogenase (LDH) leakage assay

Lactate dehydrogenase (LDH) is a marker of membrane integrity damage and an indicator of neuronal apoptosis [28]. To evaluate damaged neurons in these experiments, the release of LDH was quantitated in the culture medium using a diagnostic kit (Jiancheng Bioengineering Institute, Nanjing, China) as previously described [29]. An incubation medium before injury was collected as a pre-injury control. 30 min after the initial insult, the medium was replaced with a fresh medium to remove any LDH that was released by neurons damaged during the initial insult. Twenty-four hours later, this medium was collected for analysis of LDH.

2.9. Fluorometric TUNEL (TdT-mediated dUTP Nick end-labeling) analysis

TUNEL assays were performed using the DeadEnd™ Fluorometirc TUNEL system (Roche Applied Bioscience, Indianapolis, IN, USA) according to the manufacturer's protocol [29]. Hoechst (Sigma-Aldrich, MO, USA) staining was performed to assess the total number of cells in each well. Neurons were observed under a fluorescence microscope (Leica, Germany) using a standard fluorescein filter set. Middle regions between the scratches were analyzed. A nucleus that fluoresced green from the TUNEL staining was considered to be an apoptotic cell. The total number of neurons, which fluoresced blue from the Hoechst staining, was also determined. The ratio of apoptotic cells was calculated as an apoptotic index (AI = positive apoptotic cells/total cells × 100%), which was used to determine the apoptotic severity. At least ten high power fields were observed per well at 40×.

2.10. Calcium imaging and analysis

To determine cytosolic Ca^{2+} concentration ($[Ca^{2+}]_{cyt}$), the primary neurons were loaded with Fura-red AM (3 μM) (Life Technologies, Carlsbad, CA, USA) in an HBSS solution supplemented with 20 mM D-glucose and 10 mM HEPES (HBSS) (Gibco, MD, USA) for 45 min, and equilibrated for 30 min in the dark. To assess ER Ca^{2+} concentration ($[Ca^{2+}]_{ER}$) and mitochondrial Ca^{2+} concentration ($[Ca^{2+}]_{Mito}$), neurons were co-transfected with the plasmids of pCMV R-CEPIA1er and pCMV CEPIA2mt (Addgene, Cambridge, MA) using Lipofectamine LTX-plus (Invitrogen, CA, USA). These plasmids are new calcium-measuring organelle-entrapped protein indicators [30]. All images were captured with a confocal laser scanning microscope (FV10i, Olympus, Tokyo, Japan), and the fluorescence changes were determined in an XYT-plane fashion at the following excitation/emission wavelengths (nm): Fura-red AM (494/505–550), pCMV CEPIA2mt (473/520), and pCMV R-CEPIA1er (559/572). The objective lens, work stage and perfusion lines were heated to 37 °C. Signals from different groups were compared using identical settings for laser power and detector sensitivity for each separate experiment. For detecting SOCE, the buffer was changed with Ca^{2+}-free HBSS with 2 μM thapsigargin (TG) for 30 min. After this incubation, 2 mM Ca^{2+} was added that contained a Ca^{2+} channel inhibitor cocktail (10 μM CNQX, 10 μM AP5, and 50 μM nifedipine), which blocks any Ca^{2+} influx from ionotropic glutamate receptors (NMDA and AMPA) and L-type VDCCs [10,12]. Ca^{2+}-insensitive fluorescence was subtracted from each wavelength before calculations to normalize fluorescence values. The values were then plotted against time and shown as F/F_0. The area under the curve (AUC), peak fluorescence and peak time were assessed for each plot. For each experiment, at least four cultured neuron coverslips prepared from three or more mice cortexes were analyzed.

2.11. Detection of mitochondrial reactive oxygen species $[ROS]_{mito}$ and mitochondrial membrane potential (MMP)

In order to detect $[ROS]_{mito}$, the primary neurons were transfected with the plasmid pMitotimer (Addgene, Cambridge, MA) using Lipofectamine LTX-plus (Invitrogen, CA, USA). pMitotimer is a recently engineered reporter gene used to assess mitochondrial content, structure, stress, and damage [31]. In order to detect MMP, neurons were loaded with tetramethylrhodamine (TMRM; 20 nM) in the same manner as with Fura-red loading. The neurons were then washed and imaged in the loading buffer. Images were acquired using a confocal laser scanning microscope at the following excitation/emission wavelengths (nm): pMitotimer green (488/518) and red (543/572) and TMRM (543/560). For the fluorescence detection of MMP, the neurons were subjected to TNI using the scratch method as described above and then treated with 1 μM trifluorocabonylcyanide phenyhydrazone (FCCP; a mitochondria uncoupler) to normalize the baseline level. Images were acquired with Olympus confocal software F10V-ASW and analyzed using ImageJ (National Institutes of Health). The level of $[ROS]_{mito}$ was shown as the ratio of red/green as previously described [31]. MMP was examined by the formula: $(F_t - F_{Fccp})$ / ($(F_t - F_{Fccp})$ in uninjured group) × 100. (F_t: average fluorescence intensities after TNI; F_{Fccp}: average fluorescence intensities after addition of FCCP).

2.12. Stereotaxic injection of lentivirus

The lentiviral vectors were delivered into the mice cortex for the in vivo studies using a stereotaxic cortical injection as described previously [32,33] with some modifications. Three cortical injections were performed in the right hemisphere (ipsilateral to the lesion) as follows: point 1 (AP 0 mm, ML 2 mm from the bregma; dorsal–ventral (DV) 1.5 mm from the skull); point 2 (AP −2 mm, ML 4 mm from the bregma, DV 1.5 mm from the skull); point 3 (AP −4 mm, ML 2 mm from the bregma, DV 1.5 mm from the skull). All the target points were in the right hemisphere (ipsilateral to the lesion). Each injection contained 1.5 μl of lentivirus suspension ($1 * 10^9$ TU/ml) at a rate of 0.2 μl/min and with an additional needle retaining time for 10 min. Seven days after injection of lentivirus, mice were subjected to TBI using the CCI method as described above.

2.13. Analysis of contusion size

After deeply anesthetizing the mice, the animals were perfused with pre-cold PBS plus 0.01% heparin followed by 4% paraformaldehyde in PBS transcardially. The brains were then removed and post-fixed in 4% paraformaldehyde overnight at 4 °C. The brains were then cryoprotected in 30% sucrose for twenty-four hours before cutting coronal slices (20 μm) with a freezing microtome (Leica, Wetzlar, Germany) at 400 μm intervals throughout the brain hemispheres. Four sections were obtained at each interval, mounted onto a glass slide, and stained with 0.1% cresyl violet. Histological lesion areas were quantified with ImageJ analysis program, and lesion areas were then integrated to obtain total lesion volume in cubic millimeters.

2.14. Rotarod test

The standard rotarod test was performed to evaluate the neurological impairment, as it has been extensively used to assess rodent brain trauma with high effectivity and reliability [5,34]. Briefly, the rotarod consists of a tiltable five-lane digital-control platform and a motorized cylinder controlled by software which accelerates the platform linearly until the animal falls off (Ugo, Varese, Italy). Mice were trained on the rotarod platform at a speed of 18 rpm for 4 days in the acceleration mode (0–18 rpm/90 s) prior to CCI. Every mouse was tested for three trials with an internal of 10 min between each trial. Pre-injury baselines were obtained on the rotarod 1 h before CCI. Scores were measured as the time successfully spent running on the rotarod. After the injury, each mouse was measured at three time-points (1, 3, and 5 d after CCI). The scores were normalized to the scores of the sham group before CCI.

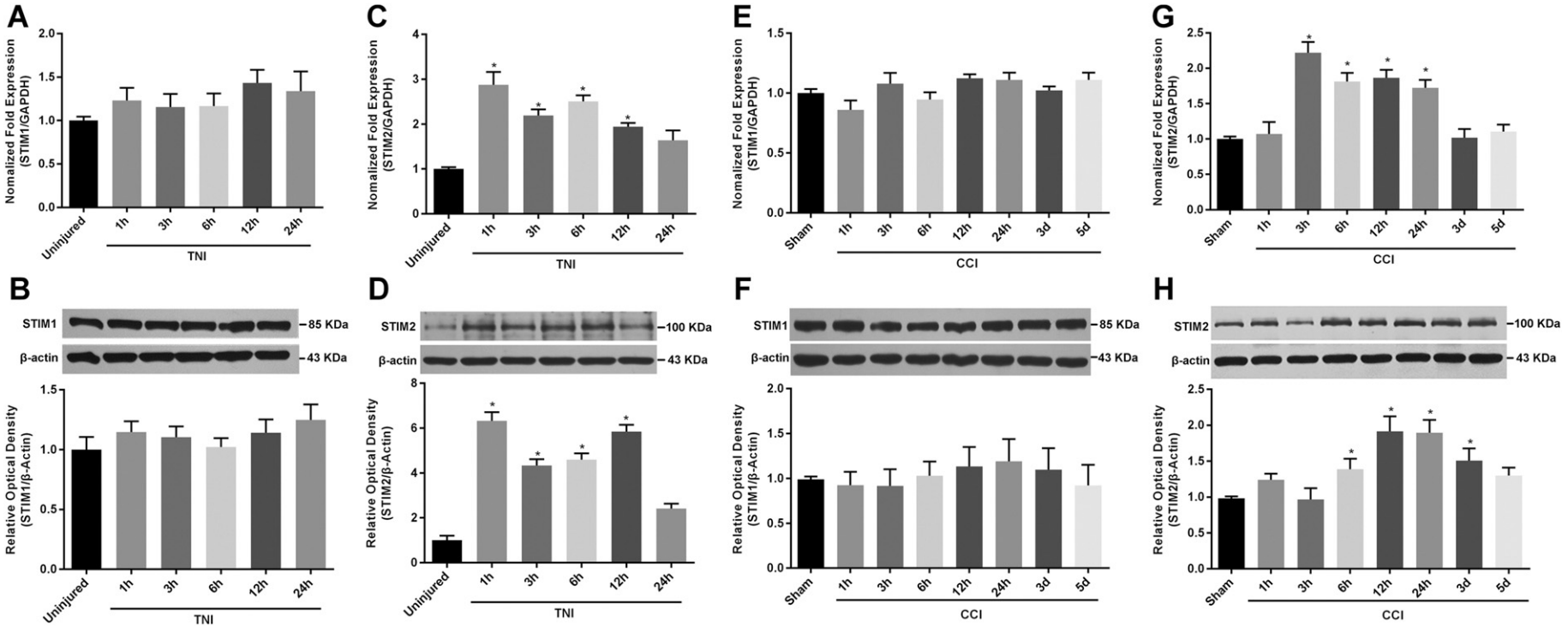

Fig. 1. Differential expression of STIM proteins after experimental TBI in vitro and in vivo. The STIM proteins in primary cultured cortex neuron were detected after TNI at different timepoints by qRT-PCR and Western blot. Relative expressions of STIM1 mRNA (A) and protein (B) were not significantly altered after TBI. However, relative expressions of STIM2 mRNA (C) and protein (D) were increased. The STIM proteins in the brain cortex ipsilateral to CCI were evaluated after experimental TBI for different timepoints by qRT-PCR and Western blot. Sham-injured mice were used as a control. Relative expressions of STIM1 mRNA (E), protein (F) were not changed significantly. However, relative expressions of STIM2 mRNA (H) and protein (I) were increased in the injured cortex. Data are means ± SEM; *, $p < 0.05$ vs. uninjured group, in vitro, n = 4; *, $p < 0.05$ vs. sham group, and in vivo, n = 7 for each group.

2.15. Statistical analysis

All of the experiments were performed at least three times. The values were expressed as a mean ± SEM, and analyzed by ANOVA followed by Bonferroni's multiple comparisons or unpaired t-test with SPSS 22.0 statistical software (IBM, Armonk, New York, USA). $p < 0.05$ was considered to be statistically significant.

3. Results

3.1. Upregulation of STIM2 expression, but not STIM1, induced by TBI in vitro and in vivo

STIM1 and STIM2 have crucial, but different roles in regulating SOCE. To examine the effect of TBI on STIM expression, a traumatic neuronal injury (TNI) was induced in cultured primary mice neurons using a scratch method, and changes in STIM1 and STIM2 mRNA expression and protein levels were determined using qRT-PCR and Western blot. The mRNA and protein from these cells were harvested at 1, 3, 6, 12, and 24 h post-TNI. Both the mRNA (Fig. 1C) and protein levels (Fig. 1D) of STIM2 were significantly elevated at 1, 3, 6, and 12 h post-TNI. STIM1 mRNA and protein levels were not affected (Fig. 1A and B).

In order to assess these results in vivo, TBI was induced in mice using a controlled cortical injury (CCI) model. The cortexes ipsilateral to the injury were used for qRT-PCR and Western blot analyses. In agreement with the in vitro data, the mice also had upregulated expression of STIM2 mRNA (Fig. 1H) and elevated protein levels (Fig. 1I). The mRNA was upregulated at 3, 6, 12, and 24 h post-CCI (Fig. 1H) and the protein levels were increased at 6, 12, 24 h and 3 d post-CCI (Fig. 1, I). Again, as with the in vitro data, STIM1 levels were unchanged (Fig. 1E, F). Therefore, we conclude that TBI induces the upregulation of STIM2 expression, but not STIM1, both in vitro and in vivo.

3.2. Knockdown of STIM2 protects against TNI-induced neuronal injury

In order to further elucidate the role of STIM1 and STIM2 in TNI-induced neuronal injury, we constructed STIM1 and STIM2 lentivirus-based RNAi vectors to downregulate the expression levels of both genes independently. Downregulation of both the mRNA and protein for both genes was confirmed using real-time RT-PCR and Western blot analyses. As shown in Fig. 2A, transfection of either STIM1-shRNA or STIM2-shRNA for 72 h significantly downregulated mRNA level by approximately 80% compared with those of normal and the Scr-shRNA groups, but had no effects on expression of either STIM gene, indicating the specificity of the shRNA. Similarly, protein levels were also knocked-down as determined by Western blot assay (Fig. 2B and C). Consistent with previous studies, our scratching model of TNI significantly increased LDH release and the apoptosis index in un-transfected (data

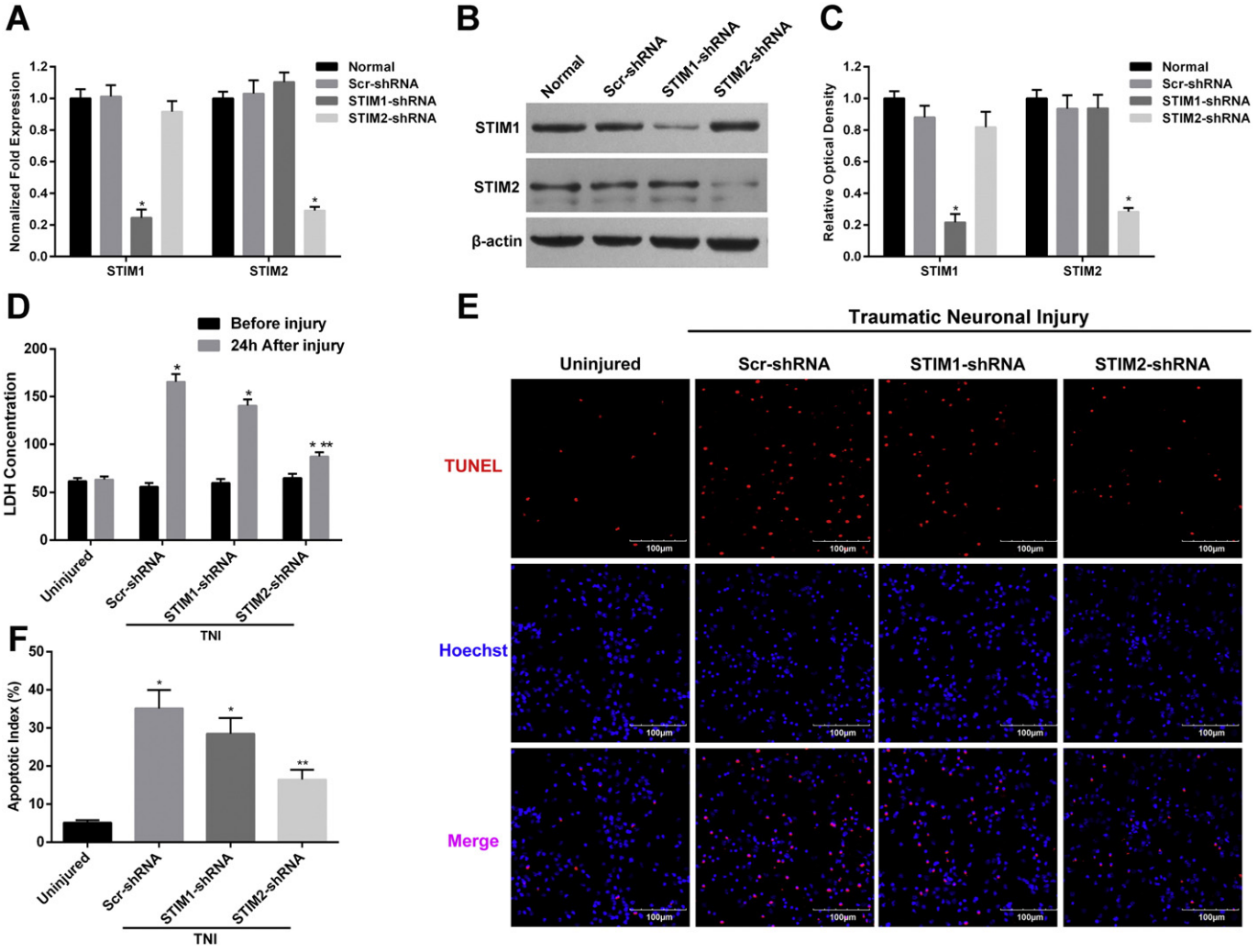

Fig. 2. Downregulation of STIM2 improves neuronal survival after TNI in vitro. After infection of Scr-shRNA, STIM1-shRNA or STIM2-shRNA for 48 h, the efficiency of downregulation was assessed for both the mRNA (A) and protein levels (B and C). After infection with lentivirus particle for 72 h and subjected to TNI for 24 h, the neuronal viability was assessed by LDH assay (D), and the neuron apoptosis was detected by TUNEL staining (E: red, TUNEL-positive; blue, Hoechst). The apoptotic index was then calculated (E). Neurons in the uninjured group were not subjected to lentiviral infection or injury. Data are means ± SEM; *, $p < 0.05$ vs. normal or uninjured group, and **, $p < 0.05$ vs. Scr-shRNA + TNI group, n = 4. Scale bars = 100 μm.

not shown) and Scr-shRNA treated cells (Fig. 2D, columns 3 and 4, and Fig. 2E and F, column 2 for both). Interestingly, downregulation of STIM2 with shRNA significantly alleviated TNI-induced neuron injury, including decreasing LDH release (Fig. 2D, columns 7 and 8) and reducing the apoptosis index (Fig. 2E and F, columns 4 for both). Downregulation of STIM1 seemed to slightly alleviate TNI-induced neuronal injury, but these results were not statistically significant (Fig. 2D, columns 5 and 6, and Fig E and F, column 3 for both). Cells that were not injured were included as controls (Fig. 2D, columns 1 and 2, and Fig. 2E and F, column 1 for both). Non-transfected cells subjected to TNI were not statistically different from cells transfected with Scr-shRNA, so they were omitted from the graphs. Taken together, these results indicate that downregulation of STIM2 attenuated TNI-induced neuronal injury.

3.3. Knockdown of STIM2 alleviated the calcium overload induced by TNI

Accumulating evidence has demonstrated that STIM1 and STIM2 have crucial roles in neuronal calcium homeostasis. Moreover, calcium disturbance is one important injury mechanism of TBI. Therefore, to understand the impact of STIM1 or STIM2 on calcium dynamics, we used shRNA knockdown of both STIM genes in cultured primary mice cortex neurons, and measured intracellular calcium dynamics using live-cell imaging with the fluorescent dye Fura-red. As shown in Fig. 3A, compared with that of uninjured normal group, TNI treatment significantly increased intracellular calcium levels in the Scr-shRNA transfected cells as indicated by an increased area under the curve (AUC) (Fig. 3B) and peak F/F_0 (Fig. 3C). Compared with Scr-shRNA group, STIM1 and STIM2 shRNA significantly reduced AUC (Fig. 3B); however, STIM2 downregulation also significantly decreased the peak F/F0 (Fig. 3C) and peak time (Fig. 3D). From these results, we conclude that while both STIM1 and STIM2 affected the TNI-induced intracellular calcium disturbance, STIM2 might play the primary roles in cortical neurons.

3.4. Knockdown of STIM2 alleviated calcium release and entry induced by TNI

In previous studies, we have found that both calcium release and calcium entry affect neuronal injury. Additionally, SOCE is a dynamic calcium regulating mechanism for calcium release and entry. Therefore, we wanted to further evaluate the effects of SOCE on TNI-induced calcium disturbance. Consistent with previous studies of SOCE in neurons, treatment of TG induced a significant calcium release in the absence of extracellular Ca^{2+}, followed by calcium entry immediately after restoration of extracellular Ca^{2+} in uninjured neurons (Fig. 4A and B). This suggests the existence of SOCE in cortex neurons. After TNI treatment, calcium release was significantly delayed as compared with uninjured controls (Fig. 4A and E), despite similar calcium entry (Fig. 4B, F, G and H). To reduce other channels' effects on calcium entry and evaluate the role of SOCE in TNI, a Ca^{2+} channel inhibitor cocktail (10 μM CNQX, 10 μM AP5, and 50 μM nifedipine) was added to the media. This cocktail inhibits diverse calcium processes involved in TNI, including NMDAR and AMPAR. Compared with those of TNI group, the AUC (Fig. 4F, column 3) and peak F/F_0 (Fig. 4G, column 3)of TNI-induced Ca^{2+} entry were significantly reduced in Scr-shRNA + TNI group after cocktail application (Fig. 4B), demonstrating that other Ca^{2+} channels were also involved in the TNI-induced Ca^{2+} disturbance. Downregulation of STIM1 significantly delayed the peak time (Fig. 4E, column 4) of TNI-induced Ca^{2+} release, but did not affect AUC (Fig. 4C, column 4) and peak F/F0 (Fig. 4D, column 4) when compared with those of the

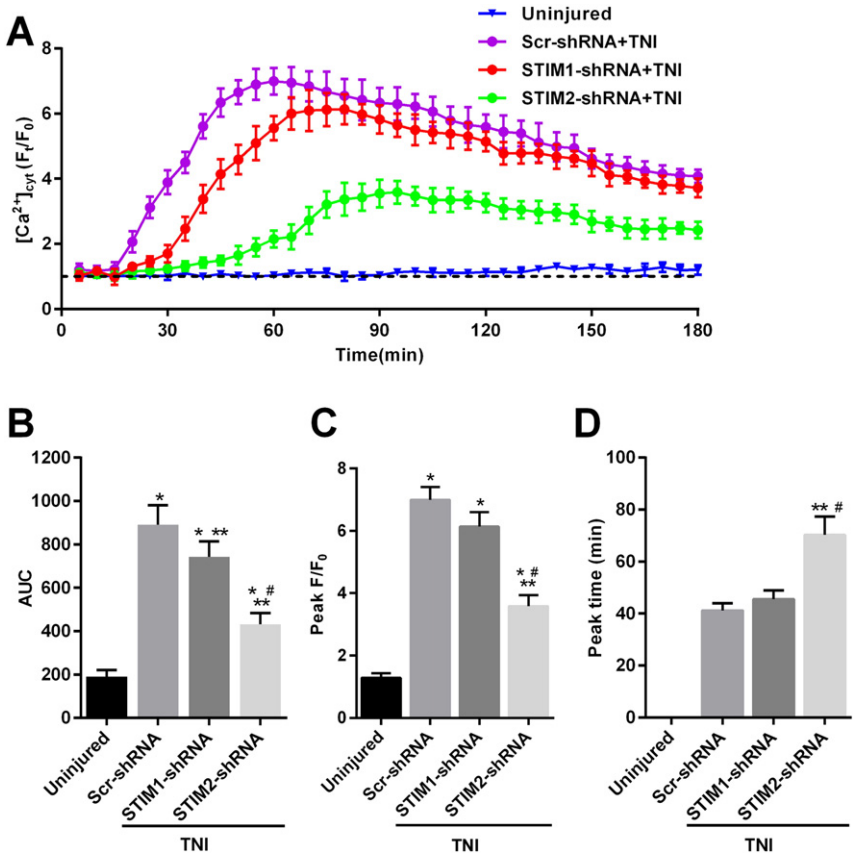

Fig. 3. Effects of STIM knockdown on intracellular Ca^{2+} concentration ($[Ca^{2+}]_{cyt}$) after TNI. The $[Ca^{2+}]_{cyt}$ was determined by the calcium indicator Fura-red. After infection with lentivirus particles for 48 h, the cortical neurons were subjected to TNI and the $[Ca^{2+}]_{cyt}$ was measured up to 3 h after injury, shown as time–series curve graph (A), area under curve (B), peak F/F_0 (C) and peak time (D). 40–50 cells were analyzed in each experiment. Neurons in the uninjured group were not subjected to lentiviral infection or injury. Data were represented as means ± SEM. *, $p < 0.05$ vs. uninjured group, **, $p < 0.05$ vs. Scr-shRNA + TNI group, #$p < 0.05$ vs. STIM1-shRNA + TNI group.

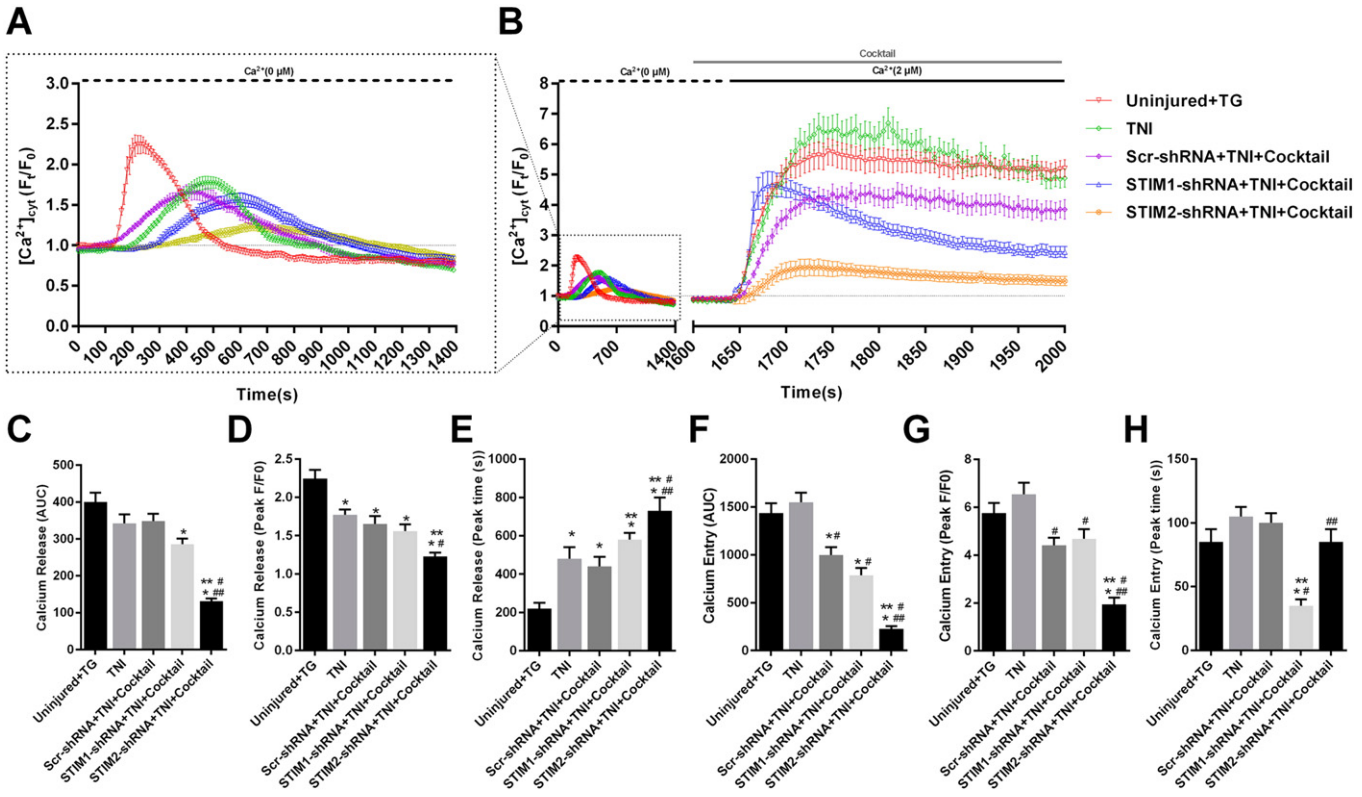

Fig. 4. Effects of STIM knockdown on Ca^{2+} release and SOCE after TNI. After infection with lentivirus for 48 h, the cells were loaded with Fura-red and baseline levels were recorded. The neurons were then insulted by TNI or 2 μM TG to release Ca^{2+} from calcium stores (black dotted line) using Ca^{2+}-free buffer. The cocktail was subsequently added into the buffer (gray full line) for 5 min in the cocktail-included group and the buffer was semi-refreshed with Ca^{2+} buffering (black full line) supplemented with cocktail or not according to experimental group. Ca^{2+} release was shown as time–series curve (A) and assessed as area under curve (C), peak F/F_0 (D) and peak time (E). Ca^{2+} entry was shown as time–series curve (B, a miniature version of figure A is included in the dotted box for reference) and assessed as area under curve (F), peak F/F_0 (G) and peak time (H). 40–50 cells were analyzed in each experiment. Data were represented as means ± SEM. $^{*}p < 0.05$ vs. uninjured + TG group, $^{\#}p < 0.05$ vs. TNI group, $^{**}p < 0.05$ vs. Scr-shRNA + TNI group, $^{\#\#}p < 0.05$ vs. STIM1-shRNA + TNI group.

Scr-shRNA TNI group. Additionally, downregulation of STIM2 significantly reduced both AUC (Fig. 4C, column 5) and peak F/F0 (Fig. 4D, column 5), as well as delaying the peak time (Fig. 4E, column 5) of TNI-induced Ca^{2+} release as compared with the Scr-shRNA group. Further, calcium entry was also evaluated in cells with STIM1 knocked-down, as compared with the scrambled controls (Fig. 4B). STIM1 knockdown decreased the peak time (Fig. 4H, column 4) of Ca^{2+} entry; but, the AUC (Fig. 4F, column 4) and the peak F/F0 (Fig. 4G, column 5) was not affected. Downregulation of STIM2 significantly decreased the AUC (Fig. 4F, column 5) and peak F/F0 (Fig. 4G, column 5), and delayed the peak time (Fig. 4H, column 5) compared with that of Scr-shRNA TNI and STIM1–shRNA group. Taken together, these results further demonstrate that STIM2 might be a key mediator of TBI-induced calcium release and entry.

3.5. Knockdown of STIM2 alleviated mitochondrial calcium overload and ER calcium release induced by TNI

After determining the role of STIM2 in TNI induced calcium release and entry, we further investigated the change of mitochondrial buffering and ER calcium release, both of which are important components of cellular calcium homeostasis. We used recently developed genetically encoded Ca^{2+} indicators (pCMV R-CEPIA1er and pCMV CEPIA2mt), which can be utilized for intraorganellar Ca^{2+} imaging. This technique provides the unique advantage of simultaneously detecting mitochondrial and ER Ca^{2+} levels with high sensitivity. As shown in Fig. 5A and B, mitochondrial calcium buffering was not significantly different among any of the groups tested in the absence of extracellular calcium. However, downregulating STIM2 expression significantly decreased ER calcium release as compared with that of Scr-shRNA TNI group (Fig. 5C and D). Although STIM1 knockdown also reduced ER calcium release as compared with the Scr-shRNA TNI group, this difference was not statistically significant (Fig. 5C and D). Once extracellular calcium was restored, mitochondrial calcium levels immediately increased in the scrambled control group by 2.51 fold over the normal level. Interestingly, downregulation of STIM2, but not STIM1, attenuated the increase of mitochondrial calcium levels, such that it was only 1.42 fold over of normal level (Fig. 5A and C). A similar effect was seen in the ER, however, there only was a slight and instant increase of ER calcium after extracellular restoration (Fig. 5C). Additionally, treatment of FCCP, which was a mitochondria uncoupler, and has shown neuroprotective roles in TBI, reduced TNI induced mitochondrial calcium overload (Fig. 5A), but had no significant effect on ER calcium (Fig. 5C). These results demonstrated that downregulation of STIM2 alleviated TNI induced mitochondrial calcium overload and ER calcium release.

3.6. Knockdown of STIM2 improved the mitochondrial dynamics and dysfunction induced by TNI

After confirming the effects of STIM2 downregulation on cellular calcium, we further studied whether the downregulation of STIM2 would affect mitochondrial function, as mitochondrial dysfunction plays a central role in TBI. To determine changes in mitochondrial morphology, ROS production, and mitochondrial damage, primary cortex neurons were first infected with a lentivirus vector at division (DIV) 4, followed by transfection with a pMitoTimer Reporter Gene at DIV6 as previously described. The cells were then subjected to TNI at DIV8. Twenty-four hours after injury, TNI induced significant mitochondrial fragmentation (Fig. 6A and B) and ROS overproduction (Fig. 6 A and C). Downregulation of STIM2 attenuated mitochondrial fragmentation (Fig. 6A and B) and ROS overproduction (Fig. 6A and C) as compared with those of the Scr-shRNA group. This suggests that STIM2 mediated

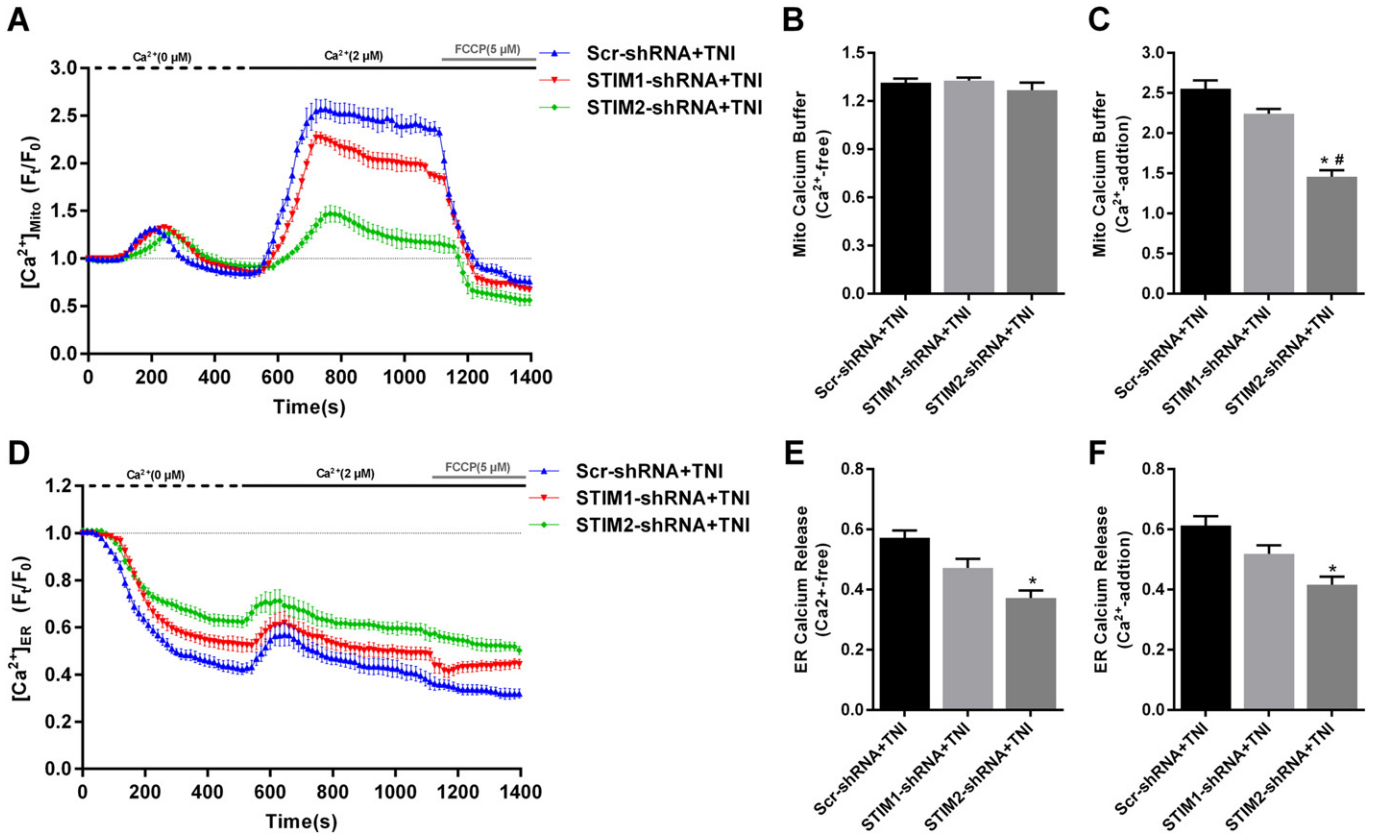

Fig. 5. Effects of STIM knockdown on mitochondrial Ca^{2+} uptake and ER Ca^{2+} release after TNI. After infection with lentivirus for 48 h, neurons were co-transfected with the plasmids of pCMV CEPIA2mt (green, Mito Ca^{2+} indicator) and pCMV R-CEPIA1er (red, ER Ca^{2+} indicator) for 24 h, and mounted on a confocal laser scanning microscope for Ca^{2+} imaging. Mitochondrial Ca^{2+} was analyzed as time–series curve graph (A) and peak F/F_0 (B, Ca^{2+}-free; C, Ca^{2+}-addition). ER Ca^{2+} was analyzed as time–series curve graph (D) and peak F/F_0 (E, Ca^{2+}-free; F, Ca^{2+}-addition). 30–40 neurons were analyzed in each experiment. Data were represented as means ± SEM. $^{*}p < 0.05$ vs. Scr-shRNA + TNI group, $^{\#}p < 0.05$ vs. STIM1-shRNA + TNI group.

SOCE might have some effects on mitochondrial morphology and ROS production in TBI. Furthermore, TNI triggered a significant loss of MMP (Fig. 6 D) and a reduction of ATP synthesis (Fig. 6E) in Scr-shRNA group. STIM2 downregulation significantly attenuated both the loss of MMP (Fig. 6D) and the decrease in ATP synthesis (Fig. 6E). STIM-1 knockdown slightly improved mitochondrial dysfunction as compared with scramble controls, but again, this result was not significant. Taken together, these data indicate that STIM2 downregulation might have a protective role in TBI-induced mitochondrial dysfunction, including protecting against mitochondrial fragmentation, ROS overproduction, loss of MMP and impairment of ATP synthesis.

3.7. Knockdown of STIM2 reduced brain damage and improved sensorimotor deficit recovery after TBI

To further assess the role of STIM2 in secondary brain injury after trauma, we knocked down the expression of STIM2 in vivo, using intracranial injection of STIM2-shRNA lentiviral vectors into the cortex of mice. Seven days after the injection of the shRNA, mice were subjected to TBI, using a controlled cortical injury (CCI) as before. Sham-operated animals that did not receive TBI were included as controls. As compared with Scr-shRNA group, STIM2-shRNA injected mice have a decreased apoptosis rate (Fig. 7A and B) and brain injury volume (Fig. 7C), suggesting an important role of STIM2 in promoting secondary brain injury, although this neuroprotection was not as profound as in the primary neuronal cultures, which might due to the limited efficacy of lentivirus infection in vivo. Behavioral deficits were also assessed using a standard rotarod test as before. Mice injected with the scrambled control had significant impairments in sensorimotor functions compared with sham group. These animals gradually recovered up to 45% of their sensorimotor function by day 3 post-injury (Fig. 7D). STIM2 knockdown significantly improved the sensorimotor function recovery after TBI (Fig. 7D), highlighting the critical role of STIM2 in promoting behavioral deficits, as well as apoptosis rate and injury volume, after TBI.

4. Discussion

The present studies have established a novel role of SOCE in TBI, affecting intracellular calcium homeostasis, and altering cytoplasmic, mitochondrial and ER calcium dynamics, as well as mitochondrial function. In addition to this, we found that TBI upregulated the expression of STIM2, without affecting STIM1 expression. Using knockdown studies, we demonstrated that the downregulation of STIM2 alleviated TBI-induced ER calcium release and calcium entry, both of which might contribute to TNI-induced neuronal calcium overload, and also decreased the mitochondrial calcium level. Furthermore, mitochondrial dysfunction triggered by TNI was improved after STIM2 knockdown. Therefore, given the calcium homeostasis disturbance and mitochondrial dysfunction are both crucial pathogenic mechanisms of secondary injury of TBI, different therapeutic drugs or strategies which target STIM2 or STIM2-mediated SOCE might contribute to develop new therapeutic protocols of TBI.

SOCE, a crucial regulating mechanism of cellular calcium homeostasis, was dynamically regulated by STIM proteins, namely STIM1 and STIM2 [8]. In the present study, STIM2, but not STIM1, was significantly upregulated in both a mechanical scratch model in vitro and a CCI model in vivo. Previous studies have demonstrated that the dysregulation of STIM expression was involved in other neurological diseases [10,15,35,36]. For example, no alteration of STIM1 was reported in sensory neurons of a painful nerve injury model or a model of Parkinson's disease (PD) [16,37], which is consistent with our studies. However, Li Y et al.'s study using a brain diffuse axon injury model did suggest

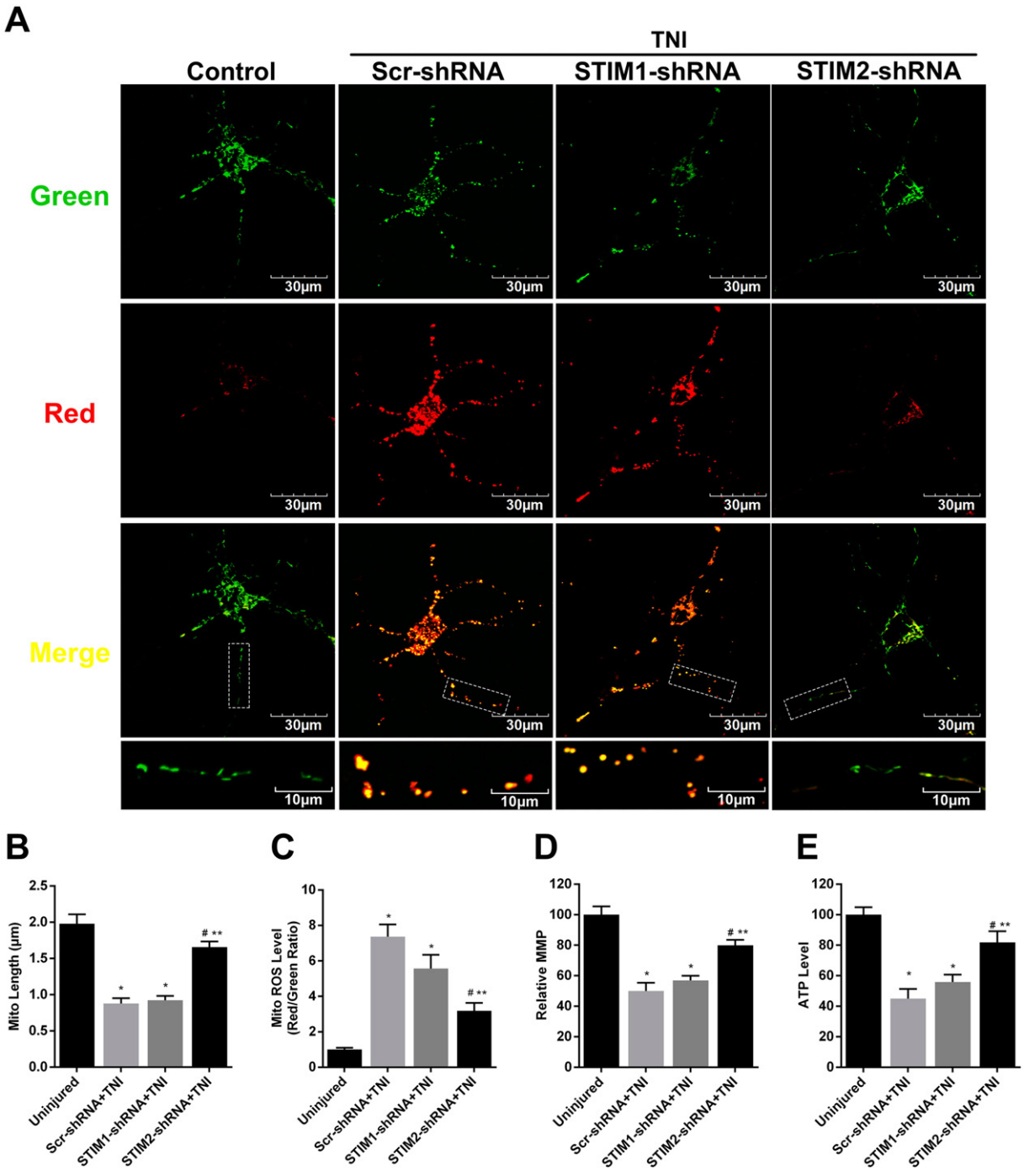

Fig. 6. Effects of STIM knockdown on mitochondrial morphology and dysfunction after TNI. Neurons were infected with lentivirus particles for 48 h. To visualize mitochondrial morphology and oxidative stress level, neurons were transfected with pMitotimer 24 h before TNI treatment. Representative confocal images of mitochondrial morphology and oxidative stress (A, green, non-oxidative levels; red, oxidative levels; the lowest images were the amplification of area in dotted box) and quantification of mitochondrial length (B) and mitochondrial oxidative levels (C) in pMitotimer positively transfected primary mouse cortex neurons. Scale bar, 30 μm in upper images, and 10 μm in the lowest images. 40–50 neurons were analyzed per group. Measurements of MMP (D) and ATP (E) are shown. 250–270 neurons were analyzed per group. Data were represented as means ± SEM from four experiments. $^{*}p < 0.05$ vs. Scr-shRNA + TNI group, $^{\#}p < 0.05$ vs. STIM1-shRNA + TNI group.

that STIM1 was highly and instantly upregulated after injury [38]. In a model of chronic epilepsy, both STIM1 and STIM2 are both increased in the hippocampus [15], while in an Alzheimer's disease (AD) model, Sun Suya et al. found reduced STIM2 expression [10]. Taken together, these studies suggest that different cell distribution and microenvironments found in these different models, as well as in different brain regions, when coupled with the diverse subcellular localization of STIM proteins allow for differential regulation of the STIM proteins. These differences also allow STIM proteins to play different roles in neurological diseases. Therefore, more attention should be paid to explore the underlying mechanisms of the STIM proteins.

Currently, the role of STIM proteins in nervous system is intensively being investigated, not only in pathological conditions, but also in physiological conditions. Physiologically, native STIM-mediated SOCE is involved in maintaining cellular calcium homeostasis [13,39,40], regulating gene expression and proliferation [11,12], affecting growth cone turning [41] and synaptic plasticity [42,43]. Unquestionably, abnormal STIM-mediated SOCE also participates in pathogenic mechanism of

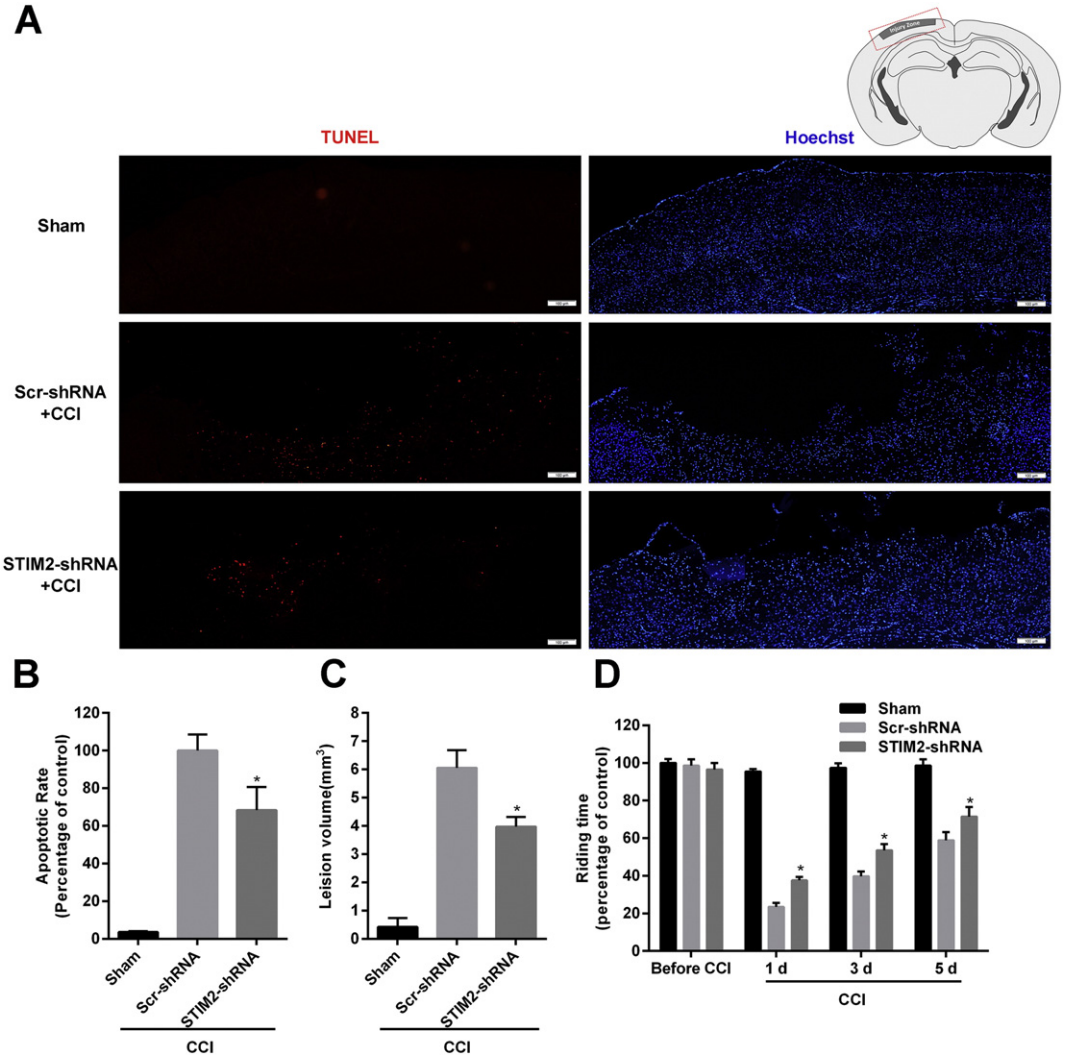

Fig. 7. Downregulation of STIM2 reduced neuronal apoptosis, decreased brain lesion volume and improved neurological deficit recovery after TBI. Mice were injected with lentivirus particle, followed by CCI. The CCI injury zone (gray box) and microscope imaging zone (red dotted box) were shown in the sketch map of a coronal section of the mice brain (A). 3 d after TBI, the apoptotic rate was assessed (A and B). n = 3 for each group, scale bar = 100 μm. Lesion volume was measured 7 d post-TBI by cresyl violet staining (C). Neurological deficits were assessed using a standard rotarod test (D). n = 5 (sham group), 5 (Scr-shRNA group), and 6 (STIM2-shRNA group). *$p < 0.05$ vs. Scr-shRNA + CCI group.

neurological diseases, like cerebral ischemia [14], AD [44], PD [45] and amyotrophic lateral sclerosis (ALS) [46]. In the current study, we also found that downregulation of STIM2, but not STIM1, alleviated TBI-induced neuron injury, in agreement with a previous study of cerebral ischemia [14]. The functional differences between STIM1 and STIM2 have also been found in different conditions, including in several disease models [14,17,47]. For example, the downregulation of STIM1 alleviated neuronal injury from oxidative stress [48,49] and ischemia injury [47], while decreased STIM2 expression or impaired SOCE were observed in AD [10] and PD [37]. Additionally, restoration of SOCE rescued mushroom spine loss [10] and increased neuron survival in a model of PD [37].

Previous studies found that the relative expression levels of STIM proteins varied by cell type, and even varied in neurons of different brain regions [14,50]. It is also known that STIM2 has a lower sensitivity to ER calcium stores and slower oligomerization rate than STIM1 [51]. These differences cause different SOCE signals between the two proteins, which leads to diverse downstream signaling. The differences between STIM1 and STIM2 expression patterns might explain the differences found in diseases related to these two proteins. Additionally, STIM1 and STIM2 have recently been implicated as intracellular signaling regulating molecules [52]. Therefore, STIM1 and STIM 2 may activate different downstream signaling cascades, triggering different molecular events, which may also explain differences between the roles of these two proteins. As very little is currently understood about the role of the STIM proteins in signaling events, much still needs to be done to elucidate about the role and difference of STIM1 and STIM2. In this paper, we have helped further understand the role of STIM2 by demonstrating that STIM2-mediated SOCE had a pathological role in TBI, and more efforts should pay to clarify the difference between STIM1 and STIM2 in TBI and other diseases.

Calcium homeostasis and signaling is extensively involved in neurological diseases, including TBI. Our results determined that downregulation of STIM2 reduced TBI-induced intracellular calcium overload, ER calcium release and mitochondrial calcium uptake. Previous studies indicated that both calcium influx from ionotropic glutamate receptor (NMDA) activation and calcium release from the ER from metabotropic glutamate receptor (mGluR1) activation contributed to secondary injury of TBI [19,53,54]. Additionally, our studies found that Ca^{2+} influx occurred through other calcium channels after TNI, and that after STIM2 downregulation, TBI-induced calcium release was attenuated. This phenomenon might due to decreasing ER calcium stores as the result of downregulation of the refilling mechanism. Furthermore, decreasing TBI-induced SOCE was also observed after STIM2 knockdown. Both decreasing calcium ER release and reducing SOCE might have contributed to attenuating TNI-induced cell calcium overload after STIM2

knockdown. These results are in agreement with a previous study in cerebellar Purkinje neurons, which established that SOCE controlled mGluR1 related Ca^{2+} signaling by affecting ER calcium [13]. Together, these data might demonstrate that STIM2 is an essential regulator of SOCE in cortex neurons.

Accumulating evidence has indicated that mitochondrial dysfunction plays an important role in TBI. In this study, we established a novel mechanistic linker among SOCE, mitochondrial dynamics and dysfunction in cortex neurons. Our study found that experimental TNI elicited mitochondrial fragmentation, ROS overproduction, MMP loss and ATP metabolism dysfunction in consistency with the study on glutamate excitotoxicity [55]. Downregulation of STIM2 rescued mitochondrial fragmentation, reduced ROS level and MMP loss, and finally improved ATP metabolism dysfunction. Normal mitochondrial morphology highly affects mitochondrial function (like ROS production, MMP maintaining and ATP synthetizing), which depended on native mitochondrial fission/fusion dynamics [56]. MFN2, a crucial regulating protein of mitochondrial fusion, is associated with TBI and regulates STIM1 trafficking and SOCE [57–59]. Wang et al. demonstrated that MFN2 was involved in glutamate-induced mitochondrial fragmentation and dysfunction via calpain-mediated MFN2 degradation, a crucial injury mechanism in secondary injury of TBI [55]. Consistent with this, our study also observed that MFN2 expression was downregulated 12 h after TBI (data not shown). Recent evidence found that SOCE regulated protein expression and degradation in neurons [11,12]. Therefore, the effects of STIM2 on mitochondrial dynamics might be regulated through MFN2; however, the exact mechanisms need to be further clarified. Additionally mitochondrial Ca^{2+} also plays a critical physiological role in regulating mitochondrial dynamics, cellular energy metabolism and signaling, and its overload contributes to various pathological conditions including neuronal apoptotic death in neurological diseases. Some studies have found that SOCE affected mitochondrial Ca^{2+} uptake [57], and extensive communication and crosstalk existed among intracellular, ER and mitochondrial Ca^{2+}. As our study also found that STIM2 knockdown led to a significant inhibition of TNI-induced mitochondrial overload, it is also possible that knocking down or inhibiting STIM2 might attenuate TNI-induced mitochondrial fragmentation and dysfunction by regulating Ca^{2+} signaling.

In conclusion, this study provided experimental evidences that STIM2 is involved in TBI-induced calcium homeostasis disturbance and mitochondrial dysfunction, promoting secondary brain injury. Downregulation of STIM2 showed a neuroprotective role in TBI. These results might contribute to the further understanding of the pathophysiological mechanisms and develop new therapeutic strategies. The two main aspects about STIM mediated SOCE that are most pressing to understand include: (1) the exact mechanisms in the difference roles of STIM1 and STIM2 in TBI; and (2) given emerging role of SOCE in regulating signaling pathways [11–13], determining other potential signaling or partner molecules which are involved in STIM2-induced neuronal injury.

Transparency document

The Transparency document associated with this article can be found, in the online version.

Conflict of interest

None.

Acknowledgments

We are indebted to the members of our laboratories at the Department of Neurosurgery, Xijing Hospital of the Fourth Military Medical University. The work was funded by the National Natural Science Foundation of China (No. 81430043), the National Science and Technology Major Project of China (2013ZX 09J13109-02C), the National Science and Technology Pillar Program of China (No. 2012BAI11B02), the Program for Changjiang Scholars and Innovative Research Team in University (No. IRT-14208), the Key Project of the Twelfth Five-year Plan of Scientific Research of China (AWS11J008) and the Science and Technology Project of Shaanxi (No. 2013KTCQ03-01).

References

[1] F. Tagliaferri, C. Compagnone, M. Korsic, F. Servadei, J. Kraus, A systematic review of brain injury epidemiology in Europe, Acta Neurochir. 148 (2006) 255–268 (discussion 268).
[2] J.A. Langlois, W. Rutland-Brown, M.M. Wald, The epidemiology and impact of traumatic brain injury: a brief overview, J. Head Trauma Rehabil. 21 (2006) 375–378.
[3] I. Cernak, Recent advances in neuroprotection for treating traumatic brain injury, Expert Opin. Investig. Drugs 15 (2006) 1371–1381.
[4] H. Algattas, J.H. Huang, Traumatic brain injury pathophysiology and treatments: early, intermediate, and late phases post-injury, Int. J. Mol. Sci. 15 (2013) 309–341.
[5] S.A. Novgorodov, C.L. Riley, J. Yu, K.T. Borg, Y.A. Hannun, R.L. Proia, M.S. Kindy, T.I. Gudz, Essential roles of neutral ceramidase and sphingosine in mitochondrial dysfunction due to traumatic brain injury, J. Biol. Chem. 289 (2014) 13142–13154.
[6] I.N. Singh, L.K. Gilmer, D.M. Miller, J.E. Cebak, J.A. Wang, E.D. Hall, Phenelzine mitochondrial functional preservation and neuroprotection after traumatic brain injury related to scavenging of the lipid peroxidation-derived aldehyde 4-hydroxy-2-nonenal, J. Cereb. Blood Flow Metab. 33 (2013) 593–599.
[7] L.K. Gilmer, K.N. Roberts, K. Joy, P.G. Sullivan, S.W. Scheff, Early mitochondrial dysfunction after cortical contusion injury, J. Neurotrauma 26 (2009) 1271–1280.
[8] J. Soboloff, B.S. Rothberg, M. Madesh, D.L. Gill, STIM proteins: dynamic calcium signal transducers, Nat. Rev. Mol. Cell Biol. 13 (2012) 549–565.
[9] L.S. Johnstone, S.J. Graham, M.A. Dziadek, STIM proteins: integrators of signalling pathways in development, differentiation and disease, J. Cell. Mol. Med. 14 (2010) 1890–1903.
[10] S.Y. Sun, H. Zhang, J. Liu, E. Popugaeva, N.J. Xu, S. Feske, C.L. White, I. Bezprozvanny, Reduced synaptic STIM2 expression and impaired store-operated calcium entry cause destabilization of mature spines in mutant presenilin mice, Neuron 82 (2014) 79–93.
[11] A. Somasundaram, A.K. Shum, H.J. McBride, J.A. Kessler, S. Feske, R.J. Miller, M. Prakriya, Store-operated CRAC channels regulate gene expression and proliferation in neural progenitor cells, J. Neurosci. 34 (2014) 9107–9123.
[12] J. Lalonde, G. Saia, G. Gill, Store-operated calcium entry promotes the degradation of the transcription factor Sp4 in resting neurons, Sci. Signal. 7 (2014) ra51.
[13] J. Hartmann, R.M. Karl, R.P.D. Alexander, H. Adelsberger, M.S. Brill, C. Ruhlmann, A. Ansel, K. Sakimura, Y. Baba, T. Kurosaki, T. Misgeld, A. Konnerth, STIM1 controls neuronal Ca2+ signaling, mGluR1-dependent synaptic transmission, and cerebellar motor behavior, Neuron 82 (2014) 635–644.
[14] A. Berna-Erro, A. Braun, R. Kraft, C. Kleinschnitz, M.K. Schuhmann, D. Stegner, T. Wultsch, J. Eilers, S.G. Meuth, G. Stoll, B. Nieswandt, STIM2 regulates capacitive Ca^{2+} entry in neurons and plays a key role in hypoxic neuronal cell death, Sci. Signal. 2 (2009) ra67.
[15] J.A. Steinbeck, N. Henke, J. Opatz, J. Gruszczynska-Biegala, L. Schneider, S. Theiss, N. Hamacher, B. Steinfarz, S. Golz, O. Brustle, J. Kuznicki, A. Methner, Store-operated calcium entry modulates neuronal network activity in a model of chronic epilepsy, Exp. Neurol. 232 (2011) 185–194.
[16] G. Gemes, M.L. Bangaru, H.E. Wu, Q. Tang, D. Weihrauch, A.S. Koopmeiners, J.M. Cruikshank, W.M. Kwok, Q.H. Hogan, Store-operated Ca^{2+} entry in sensory neurons: functional role and the effect of painful nerve injury, J. Neurosci. 31 (2011) 3536–3549.
[17] J. Gruszczynska-Biegala, P. Pomorski, M.B. Wisniewska, J. Kuznicki, Differential roles for STIM1 and STIM2 in store-operated calcium entry in rat neurons, PLoS One 6 (2011) e19285.
[18] W. Zeiger, K.S. Vetrivel, V. Buggia-Prevot, P.D. Nguyen, S.L. Wagner, M.L. Villereal, G. Thinakaran, Ca^{2+} influx through store-operated Ca^{2+} channels reduces Alzheimer disease beta-amyloid peptide secretion, J. Biol. Chem. 288 (2013) 26955–26966.
[19] T. Chen, F. Fei, X.F. Jiang, L. Zhang, Y. Qu, K. Huo, Z. Fei, Down-regulation of Homer1b/c attenuates glutamate-mediated excitotoxicity through endoplasmic reticulum and mitochondria pathways in rat cortical neurons, Free Radic. Biol. Med. 52 (2012) 208–217.
[20] A.G. Mukhin, S.A. Ivanova, S.M. Knoblach, A.I. Faden, New in vitro model of traumatic neuronal injury: evaluation of secondary injury and glutamate receptor-mediated neurotoxicity, J. Neurotrauma 14 (1997) 651–663.
[21] B. Morrison III, B.S. Elkin, J.P. Dolle, M.L. Yarmush, In vitro models of traumatic brain injury, Annu. Rev. Biomed. Eng. 13 (2011) 91–126.
[22] S. Margulies, R. Hicks, C.T.T. Br, Combination therapies for traumatic brain injury: prospective considerations, J. Neurotrauma 26 (2009) 925–939.
[23] Y. Zhao, P. Luo, Q. Guo, S. Li, L. Zhang, M. Zhao, H. Xu, Y. Yang, W. Poon, Z. Fei, Interactions between SIRT1 and MAPK/ERK regulate neuronal apoptosis induced by traumatic brain injury in vitro and in vivo, Exp. Neurol. 237 (2012) 489–498.
[24] P. Luo, T. Chen, Y. Zhao, L. Zhang, Y. Yang, W. Liu, S. Li, W. Rao, S. Dai, J. Yang, Z. Fei, Postsynaptic scaffold protein Homer 1a protects against traumatic brain injury via regulating group I metabotropic glutamate receptors, Cell Death Dis. 5 (2014) e1174.
[25] M. Bilgen, A new device for experimental modeling of central nervous system injuries, Neurorehabil. Neural Repair 19 (2005) 219–226.

[26] K.J. Livak, T.D. Schmittgen, Analysis of relative gene expression data using real-time quantitative PCR and the 2(-delta delta C(T)) method, Methods 25 (2001) 402–408.
[27] P. Luo, Y. Zhao, D. Li, T. Chen, S. Li, X. Chao, W. Liu, L. Zhang, Y. Qu, X. Jiang, G. Lu, W. Poon, Z. Fei, Protective effect of Homer 1a on tumor necrosis factor-alpha with cycloheximide-induced apoptosis is mediated by mitogen-activated protein kinase pathways, Apoptosis 17 (2012) 975–988.
[28] D. Lobner, Comparison of the LDH and MTT assays for quantifying cell death: validity for neuronal apoptosis? J. Neurosci. Methods 96 (2000) 147–152.
[29] F. Fei, W. Rao, L. Zhang, B.G. Chen, J. Li, Z. Fei, Z. Chen, Downregulation of Homer1b/c improves neuronal survival after traumatic neuronal injury, Neuroscience 267 (2014) 187–194.
[30] J. Suzuki, K. Kanemaru, K. Ishii, M. Ohkura, Y. Okubo, M. Iino, Imaging intraorganellar Ca^{2+} at subcellular resolution using CEPIA, Nat. Commun. 5 (2014) 4153.
[31] R.C. Laker, P. Xu, K.A. Ryall, A. Sujkowski, B.M. Kenwood, K.H. Chain, M. Zhang, M.A. Royal, K.L. Hoehn, M. Driscoll, P.N. Adler, R.J. Wessells, J.J. Saucerman, Z. Yan, A novel MitoTimer reporter gene for mitochondrial content, structure, stress, and damage in vivo, J. Biol. Chem. 289 (2014) 12005–12015.
[32] R.L. Lowery, A.K. Majewska, Intracranial injection of adeno-associated viral vectors, J. Vis. Exp. 17 (45) (2014) 1–3.
[33] A. Cetin, S. Komai, M. Eliava, P.H. Seeburg, P. Osten, Stereotaxic gene delivery in the rodent brain, Nat. Protoc. 1 (2007) 3166–3173.
[34] R.J. Hamm, B.R. Pike, D.M. O'Dell, B.G. Lyeth, L.W. Jenkins, The rotarod test: an evaluation of its effectiveness in assessing motor deficits following traumatic brain injury, J. Neurotrauma. 11 (1994) 187–196.
[35] F. Moccia, E. Zuccolo, T. Soda, F. Tanzi, G. Guerra, L. Mapelli, F. Lodola, E. D'Angelo, Stim and Orai proteins in neuronal Ca^{2+} signaling and excitability, Front Cell Neurosci. 9 (2015) 153.
[36] L. Bojarski, P. Pomorski, A. Szybinska, M. Drab, A. Skibinska-Kijek, J. Gruszczynska-Biegala, J. Kuznicki, Presenilin-dependent expression of STIM proteins and dysregulation of capacitative Ca^{2+} entry in familial Alzheimer's disease, Biochim. Biophys. Acta 1793 (2009) 1050–1057.
[37] S. Selvaraj, Y. Sun, J.A. Watt, S. Wang, S. Lei, L. Birnbaumer, B.B. Singh, Neurotoxin-induced ER stress in mouse dopaminergic neurons involves downregulation of TRPC1 and inhibition of AKT/mTOR signaling, J. Clin. Invest. 122 (2012) 1354–1367.
[38] Y. Li, J. Song, X. Liu, M. Zhang, J. An, P. Sun, D. Li, T. Jin, J. Wang, High expression of STIM1 in the early stages of diffuse axonal injury, Brain Res. 1495 (2013) 95–102.
[39] M.S. Muller, R. Fox, A. Schousboe, H.S. Waagepetersen, L.K. Bak, Astrocyte glycogenolysis is triggered by store-operated calcium entry and provides metabolic energy for cellular calcium homeostasis, Glia 62 (2014) 526–534.
[40] J.S. Xia, R. Pan, X.H. Gao, O. Meucci, H.J. Hu, Native store-operated calcium channels are functionally expressed in mouse spinal cord dorsal horn neurons and regulate resting calcium homeostasis, J. Physiol. Lond. 592 (2014) 3443–3461.
[41] C.B. Mitchell, R.J. Gasperini, D.H. Small, L. Foa, STIM1 is necessary for store-operated calcium entry in turning growth cones, J. Neurochem. 122 (2012) 1155–1166.
[42] E. Korkotian, M. Frotscher, M. Segal, Synaptopodin regulates spine plasticity: mediation by calcium stores, J. Neurosci. 34 (2014) 11641–11651.
[43] A. Baba, T. Yasui, S. Fujisawa, R.X. Yamada, M.K. Yamada, N. Nishiyama, N. Matsuki, Y. Ikegaya, Activity-evoked capacitative Ca^{2+} entry: implications in synaptic plasticity, J. Neurosci. Off. J. Soc. Neurosci. 23 (2003) 7737–7741.
[44] M.A. Leissring, Y. Akbari, C.M. Fanger, M.D. Cahalan, M.P. Mattson, F.M. LaFerla, Capacitative calcium entry deficits and elevated luminal calcium content in mutant presenilin-1 knockin mice, J. Cell Biol. 149 (2000) 793–798.
[45] J. Wu, H.P. Shih, V. Vigont, L. Hrdlicka, L. Diggins, C. Singh, M. Mahoney, R. Chesworth, G. Shapiro, O. Zimina, X. Chen, Q. Wu, L. Glushankova, M. Ahlijanian, G. Koenig, G.N. Mozhayeva, E. Kaznacheyeva, I. Bezprozvanny, Neuronal store-operated calcium entry pathway as a novel therapeutic target for Huntington's disease treatment, Chem. Biol. 18 (2011) 777–793.
[46] H. Kawamata, S.K. Ng, N. Diaz, S. Burstein, L. Morel, A. Osgood, B. Sider, H. Higashimori, P.G. Haydon, G. Manfredi, Y.J. Yang, Abnormal intracellular calcium signaling and SNARE-dependent exocytosis contributes to SOD1G93A astrocyte-mediated toxicity in amyotrophic lateral sclerosis, J. Neurosci. 34 (2014) 2331–2348.
[47] M. Zhang, J.N. Song, Y. Wu, Y.L. Zhao, H.G. Pang, Z.F. Fu, B.F. Zhang, X.D. Ma, Suppression of STIM1 in the early stage after global ischemia attenuates the injury of delayed neuronal death by inhibiting store-operated calcium entry-induced apoptosis in rats, Neuroreport 25 (2014) 507–513.
[48] B. Li, L. Xiao, Z.Y. Wang, P.S. Zheng, Knockdown of STIM1 inhibits 6-hydroxydopamine-induced oxidative stress through attenuating calcium-dependent ER stress and mitochondrial dysfunction in undifferentiated PC12 cells, Free Radic. Res. 48 (2014) 758–768.
[49] W. Rao, L. Zhang, N. Su, K. Wang, H. Hui, L. Wang, T. Chen, P. Luo, Y.F. Yang, Z.B. Liu, Z. Fei, Blockade of SOCE protects HT22 cells from hydrogen peroxide-induced apoptosis, Biochem. Biophys. Res. Commun. 441 (2013) 351–356.
[50] A. Skibinska-Kijek, M.B. Wisniewska, J. Gruszczynska-Biegala, A. Methner, J. Kuznicki, Immunolocalization of STIM1 in the mouse brain, Acta Neurobiol. Exp. 69 (2009) 413–428.
[51] P.B. Stathopulos, L. Zheng, M. Ikura, Stromal interaction molecule (STIM) 1 and STIM2 calcium sensing regions exhibit distinct unfolding and oligomerization kinetics, J. Biol. Chem. 284 (2009) 728–732.
[52] L. Majewski, J. Kuznicki, SOCE in neurons: signaling or just refilling? Biochim. Biophys. Acta 1853 (2015) 1940–1952.
[53] H.L. Cater, D. Gitterman, S.M. Davis, C.D. Benham, B. Morrison III, L.E. Sundstrom, Stretch-induced injury in organotypic hippocampal slice cultures reproduces in vivo post-traumatic neurodegeneration: role of glutamate receptors and voltage-dependent calcium channels, J. Neurochem. 101 (2007) 434–447.
[54] J. Spaethling, L. Le, D.F. Meaney, NMDA receptor mediated phosphorylation of GluR1 subunits contributes to the appearance of calcium-permeable AMPA receptors after mechanical stretch injury, Neurobiol. Dis. 46 (2012) 646–654.
[55] W. Wang, F. Zhang, L. Li, F. Tang, S.L. Siedlak, H. Fujioka, Y. Liu, B. Su, Y. Pi, X. Wang, MFN2 couples glutamate excitotoxicity and mitochondrial dysfunction in motor neurons, J. Biol. Chem. 290 (2015) 168–182.
[56] D.C. Chan, Mitochondria: dynamic organelles in disease, aging, and development, Cell. 125 (2006) 1241–1252.
[57] D. Bakowski, C. Nelson, A.B. Parekh, Endoplasmic reticulum-mitochondria coupling: local Ca(2)(+) signalling with functional consequences, Pflugers Arch. — Eur. J. Physiol. 464 (2012) 27–32.
[58] K. Singaravelu, C. Nelson, D. Bakowski, O.M. de Brito, S.W. Ng, J. Di Capite, T. Powell, L. Scorrano, A.B. Parekh, Mitofusin 2 regulates STIM1 migration from the Ca^{2+} store to the plasma membrane in cells with depolarized mitochondria, J. Biol. Chem. 286 (2011) 12189–12201.
[59] A. Quintana, M. Hoth, Mitochondrial dynamics and their impact on T cell function, Cell Calcium 52 (2012) 57–63.